Journal of Power Sources 257 (2014) 186–191

Contents lists available at ScienceDirect

Journal of Power Sources

journal homepage: www.elsevier.com/locate/jpowsour

Short communication

3-D dumbbell-like $LiNi_{1/3}Mn_{1/3}Co_{1/3}O_2$ cathode materials assembled with nano-building blocks for lithium-ion batteries

Won-Hee Ryu [a,b], Sung-Jin Lim [a], Won-Keun Kim [a], HyukSang Kwon [a,*]

[a] Department of Materials Science and Engineering, Korea Advanced Institute of Science and Technology, Daejeon 305-701, Republic of Korea
[b] Department of Chemical and Environmental Engineering, Yale University, New Haven, CT 06520-8286, United States

HIGHLIGHTS

- We develop 3-D dumbbell-like microsphere carbonate assembled with nanocubes.
- We prepare $LiNi_{1/3}Mn_{1/3}Co_{1/3}O_2$ cathode materials using similarly-shaped precursor.
- 3-D dumbbell-like $LiNi_{1/3}Mn_{1/3}Co_{1/3}O_2$ exhibits excellent electrochemical performance.

GRAPHICAL ABSTRACT

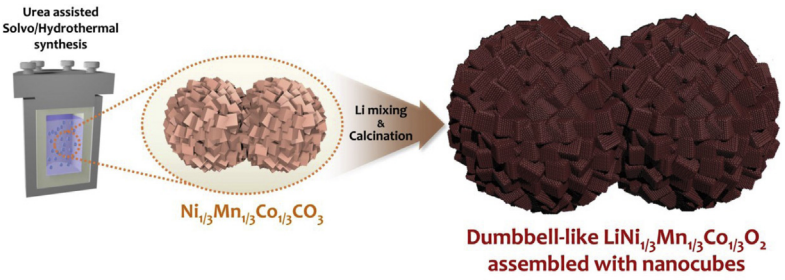

ARTICLE INFO

Article history:
Received 27 December 2013
Received in revised form
1 February 2014
Accepted 2 February 2014
Available online 10 February 2014

Keywords:
Hierarchical microsphere
Layered cathode materials
Solvo/hydrothermal method
Multi transition metal carbonate
Lithium-ion batteries
Nanomaterials

ABSTRACT

Dumbbell-like microsphere carbonate precursors including multi-transition metal components ($Ni_{1/3}Mn_{1/3}Co_{1/3}CO_3$) assembled with nano-building blocks were synthesized by urea-assisted solvo/hydrothermal method, and layered cathode materials ($LiNi_{1/3}Mn_{1/3}Co_{1/3}O_2$) were subsequently prepared using the similarly shaped carbonate precursors for Li-ion batteries. For the synthesis of hierarchical microsphere structures, the partial addition of viscous organic solvent (e.g. ethylene glycol) in aqueous solution played a crucial role, not only in suppressing the sudden particle growth but also in regulating the directional crystallization of carbonate particles on the surface. The dumbbell-like $LiNi_{1/3}Mn_{1/3}Co_{1/3}O_2$ assembled with nanocubes prepared via the urea-assisted solvo/hydrothermal method exhibited better electrochemical characteristics, such as initial discharge capacity, cyclic performance, and rate-capability as a cathode material of Li-ion batteries, compared with the $LiNi_{1/3}Mn_{1/3}Co_{1/3}O_2$ materials prepared via the conventional co-precipitation method.

1. Introduction

Because of the abrupt increase in interest in alternative fuels and renewable energy, substantial efforts have been exerted to develop electrochemical energy storage systems such as Li-ion batteries to effectively store extra energy [1–4]. Further breakthroughs in electrode materials hold the key to making significant improvements in the current Li-ion batteries [5,6]. Most of the progress in the development of cathode materials to replace conventional $LiCoO_2$ has been made by regulating the stoichiometry of transition metal sites (Mn, Ni, Co, Fe) and anion sites (F, PO_4, SiO_4, SO_4F), thereby converting the structural and electrochemical properties of the cathode materials [5,7–11]. The introduction of multiple components in the transition metal sites of cathode materials can enable high operating voltages, additional reversible capacity, and

* Corresponding author. Tel.: +82 42 350 3326; fax: +82 42 350 3310.
E-mail addresses: rwh012@kaist.ac.kr (W.-H. Ryu), hskwon@kaist.ac.kr (H. Kwon).

http://dx.doi.org/10.1016/j.jpowsour.2014.02.003
0378-7753/

improved cyclability. For example, the diverse tuning of transition metal sites (M) in layered $LiMO_2$ brought about the currently progressive layered cathodes, such as $LiNi_{0.5}Mn_{0.5}O_2$, and $LiNi_{1/3}Mn_{1/3}Co_{1/3}O_2$, by improving the operating voltage and capacity [9,12–15]. To synthesize multi-component cathode materials, the synthesis of precursors in which multiple transition metal components are atomically mixed in a hydroxide or carbonate structure is known to be essential [16,17]. The co-precipitation method, which involves a precipitate of an insoluble compound from a homogeneous transition metal solution, is well known as a conventional synthetic method for preparing multi-component metal precursors [18,19]. In other way, sol–gel method and polymer assisted method have also been reported for the synthesis of multi-component metal precursors [20,21]. However, the morphological control is limited to microspheres and is considered a hindrance to making further improvements in the electrochemical performance.

Recently, 3-D hierarchical microsphere cathodes have attracted significant interest due primarily to the fact that the nanostructured nodule surface around the core can not only increase the reaction sites with Li^+ because of it large surface area but it can also prevent the decrease in the volumetric energy density caused by the low tap-density of nanomaterials [12,22,23]. The key point to preparing a 3-D hierarchical microsphere cathode is determining how to control the shape and composition of the precursor because the final morphologies and atomic compositions of 3-D hierarchical microsphere cathodes are highly influenced by the morphological and stoichiometric feature of the precursor [22,24]. Recently, some studies related to the synthesis of 3-D hierarchical microsphere precursors have been reported [25,26]. However, the 3-D hierarchical microsphere precursors reported are mostly limited to single metal component precursors such as MnO_2 or need to be further optimized for minute morphological control [26–28].

Here, we report the novel synthesis of a dumbbell-like microsphere carbonate precursor including multi-transition metal components ($Ni_{1/3}Mn_{1/3}Co_{1/3}CO_3$) assembled with nano-building blocks by the urea-assisted solvo/hydrothermal method and subsequent preparation of layered cathode materials ($LiNi_{1/3}Mn_{1/3}Co_{1/3}O_2$) using a tailored precursor for Li-ion batteries (Fig. 1). The electrochemical performance of the dumbbell-like $LiNi_{1/3}Mn_{1/3}Co_{1/3}O_2$ assembled with nano-building blocks (nanocubes) was compared with the $LiNi_{1/3}Mn_{1/3}Co_{1/3}O_2$ prepared via the conventional co-precipitation method.

2. Experimental

2.1. Synthesis and microstructural characterization

The synthesis procedure of dumbbell-like $LiNi_{1/3}Mn_{1/3}Co_{1/3}O_2$ assembled with nanocubes (SH-NMC) consists of two steps: (1) preparation of dumbbell-like $Ni_{1/3}Mn_{1/3}Co_{1/3}CO_3$ precursors assembled with nanocubes by urea-assisted solvo/hydrothermal method and (2) synthesis of 3-D hierarchical $LiNi_{1/3}Mn_{1/3}Co_{1/3}O_2$ microsphere cathode by shape controlled carbonate precursor from (1). To obtain the $Ni_{1/3}Mn_{1/3}Co_{1/3}CO_3$ precursor, $Ni(CH_3COO)_2{\cdot}4H_2O$, $Mn(CH_3COO)_2{\cdot}4H_2O$, $Co(CH_3COO)_2{\cdot}4H_2O$ (Ni:Mn:Co = 0.333:0.333:0.333, total: 0.1 M) and NH_2CONH_2 (Urea, 2.4 g) were dissolved in mixture solution of distilled water and ethylene glycol in a 35 ml:45 ml (total volume: 80 ml) respectively and stirred with a magnetic stirrer for 6 h. The mixed solution was sealed into a Teflon-lined stainless steel autoclave and then annealed at 140 °C for 10 h. After the reaction was completed, the products were filtered and washed using distilled water and ethanol several times. They were finally dried at 100 °C overnight. As reference, $Ni_{1/3}Mn_{1/3}Co_{1/3}CO_3$ precursor was prepared by co-precipitation method as following procedure. A 0.5 M aqueous solution of NH_4HCO_3 dropped into a 0.1 M aqueous solution of Ni, Co, and Mn sulfate (Ni:Mn:Co = 0.333:0.333:0.333). The co-precipitated $Ni_{1/3}Mn_{1/3}Co_{1/3}CO_3$ precursor was filtered and dried at 100 °C overnight. The obtained $Ni_{1/3}Mn_{1/3}Co_{1/3}CO_3$ precursors were mixed with a stoichiometric amount of Li_2CO_3, followed by calcination at 700 °C for 12 h in an air atmosphere for preparing layered $LiNi_{1/3}Mn_{1/3}Co_{1/3}O_2$. The each layered $LiNi_{1/3}Mn_{1/3}Co_{1/3}O_2$ cathode materials which were obtained from the different carbonate precursors synthesized via solvo/hydrothermal method and co-precipitation were named as SH-NMC and C-NMC, respectively. Surface morphology of the samples was analyzed using scanning electron microscope (SEM, PHILIPS, XL30SFEG) and transmission electron microscope (TEM, FEI, Tecnai F30 S-Twin). The crystal structures of the samples were analyzed by X-ray diffraction (XRD, RIGAKU, D/MAX-RC). The specific surface area of the samples was analyzed by Brunauer–Emmet–Teller (BET) surface area analyzer (Micromeritics ASAP 2020 M + C).

2.2. Electrochemical characterization

To fabricate electrodes, a mixture of each active material (85 wt %) and conductive carbon (super-P, 8 wt %) was added to *N*-methyl-2-pyrrolidone (NMP) solution that contained polyvinylidene fluoride (PVDF). The slurry was pasted onto an Al current collector and then dried in a vacuum oven. Subsequently, it was punched into a 1.4 cm diameter disc shape after press. The average loading density of active materials was 1.7 mg cm^{-2}. The electrochemical properties of the prepared electrodes were evaluated by using 2032 coin-type cells that were assembled in an argon-filled glove box. A Li metal foil was used as the counter electrode and 1 M $LiPF_6$ dissolved in 1:1 (v/v) ethylene carbonate (EC) and diethyl carbonate (DEC) was adopted as an electrolyte.

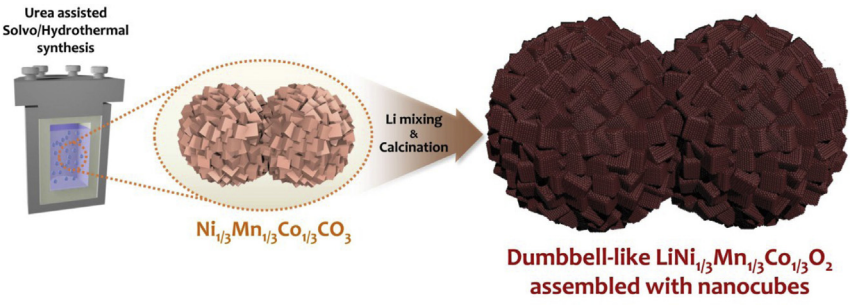

Fig. 1. Schematic illustration of sequential steps for the synthesis of dumbbell-like $LiNi_{1/3}Mn_{1/3}Co_{1/3}O_2$ layered cathode material assembled with nanocubes.

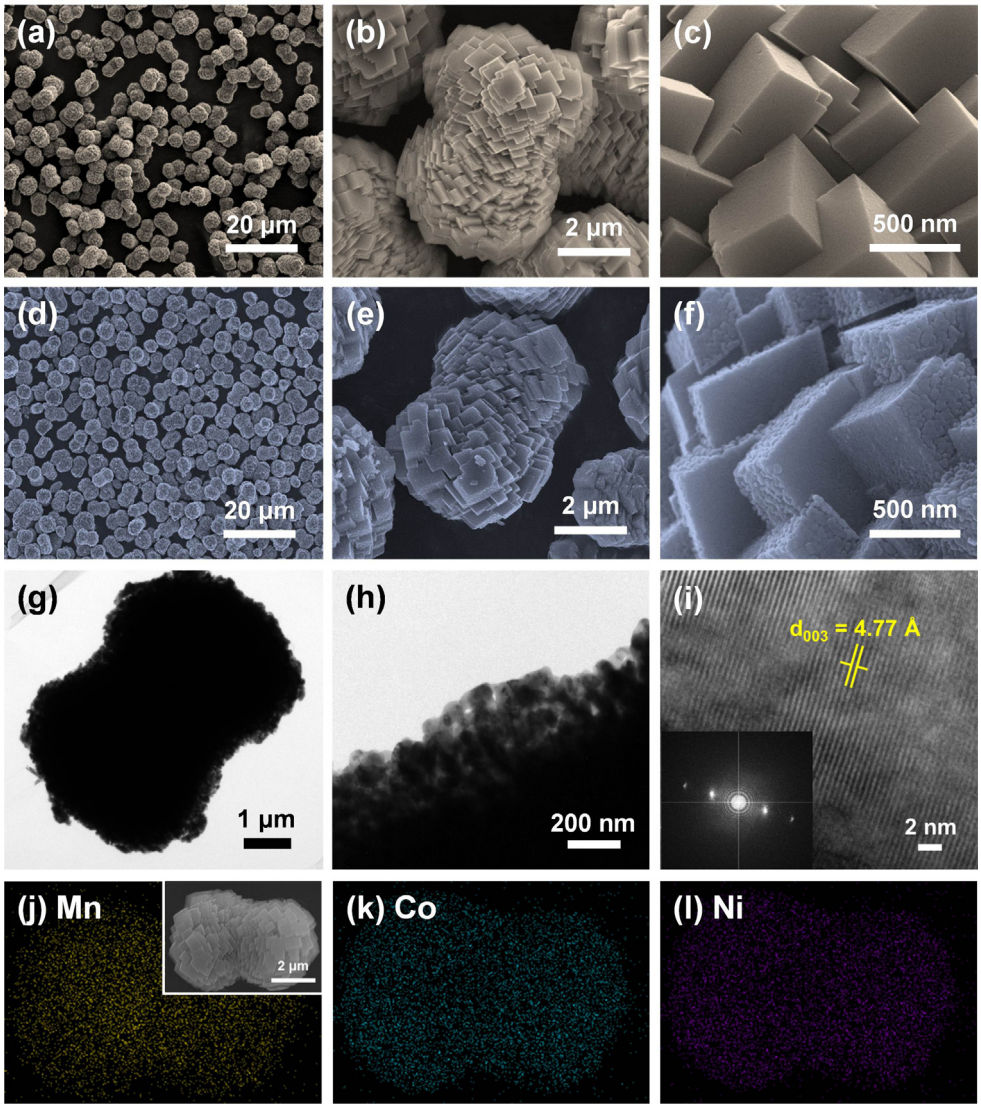

Fig. 2. (a–c) SEM images of $Ni_{1/3}Mn_{1/3}Co_{1/3}CO_3$ prepared by urea assisted solvo/hydrothermal method with different magnification; (d–f) SEM images of $LiNi_{1/3}Mn_{1/3}Co_{1/3}O_2$ obtained using the $Ni_{1/3}Mn_{1/3}Co_{1/3}CO_3$ precursor with different magnification; (g–h) HR-TEM images and (i) lattice fringe of $LiNi_{1/3}Mn_{1/3}Co_{1/3}O_2$ obtained using the $Ni_{1/3}Mn_{1/3}Co_{1/3}CO_3$ precursor. The inset figure of (i) is the corresponded FFT image; atomic distribution of (j) manganese (yellow color), (k) cobalt (cyan color), and (l) nickel (purple color) analyzed from SEM image of inset of (j). (For interpretation of the references to color in this figure legend, the reader is referred to the web version of this article.)

All electrochemical experiments were performed at room temperature.

3. Results and discussion

The multicomponent carbonate ($Ni_{1/3}Mn_{1/3}Co_{1/3}CO_3$) precursor was synthesized by the urea-assisted solvo/hydrothermal method. The chemical reaction in the urea-containing solution used to synthesize the $Ni_{1/3}Mn_{1/3}Co_{1/3}CO_3$ precursors could be described as follows: [29,30]

$$NH_2CONH_2 + H_2O \rightarrow 2NH_3 + CO_2 \quad (1)$$

$$NH_3 + H_2O \rightarrow NH_4^+ + OH^- \quad (2)$$

$$CO_2 + 2OH^- \rightarrow CO_3^{2-} + H_2O \quad (3)$$

$$0.333Ni^{2+} + 0.333Mn^{2+} + 0.333Co^{2+} + CO_3^{2-} \rightarrow Ni_{1/3}Mn_{1/3}Co_{1/3}CO_3 \quad (4)$$

$$NH_4^+ + CH_3COO^- \rightarrow CH_3COONH_4 \quad (5)$$

The reactions involve the thermal decomposition of urea and the generation of OH^- and CO_3^{2-} ions and the subsequent precipitation of $Ni_{1/3}Mn_{1/3}Co_{1/3}CO_3$ precursor under solvo/hydrothermal conditions. Fig. 2 shows the microstructural evolution of the obtained $Ni_{1/3}Mn_{1/3}Co_{1/3}CO_3$ precursor and the $LiNi_{1/3}Mn_{1/3}Co_{1/3}O_2$ synthesized using the precursor. The highly uniform $Ni_{1/3}Mn_{1/3}Co_{1/3}CO_3$ particles were obtained as shown in Fig. 2a. Interestingly, two of the spherical primary particles with a diameter of 5 μm were combined each other (like a dumbbell), and randomly oriented nanocubes were assembled on the surface (Fig. 2b). Each nanocube assembled on the spherical particle exhibited a smooth surface with an average size of 500 nm (Fig. 2c). The uniformity and morphologies of the $Ni_{1/3}Mn_{1/3}Co_{1/3}CO_3$ precursor were successfully

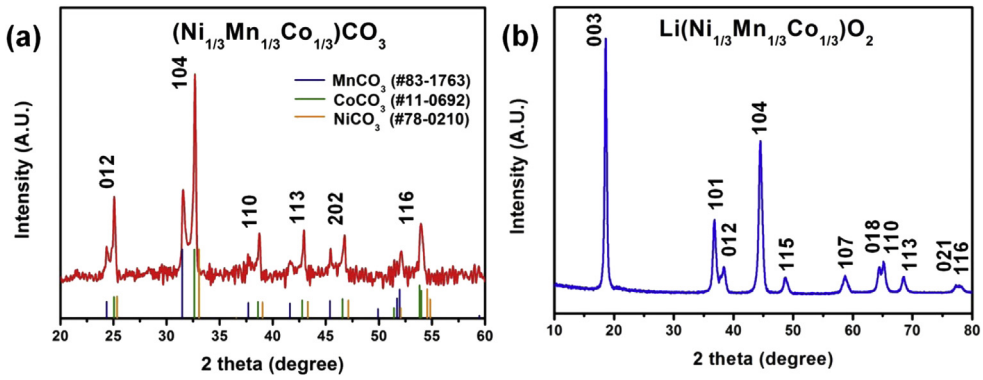

Fig. 3. X-ray diffraction patterns of (a) $Ni_{1/3}Mn_{1/3}Co_{1/3}CO_3$ prepared by urea assisted solvo/hydrothermal method and (b) $LiNi_{1/3}Mn_{1/3}Co_{1/3}O_2$ obtained using the $Ni_{1/3}Mn_{1/3}Co_{1/3}CO_3$ precursor.

controlled by replacing a suitable amount of ethylene glycol with the partial aqueous solution. The addition of viscous ethylene glycol in the aqueous solution can suppress the sudden particle growth and regulate the directional crystallization of $Ni_{1/3}Mn_{1/3}Co_{1/3}CO_3$ precursor on the surface because the diffusivity of metal ions in a viscous solution is decreased according to the Stokes–Einstein relation ($D \propto 1/\eta$, D: diffusion constant, η: solution viscosity).

After mixing with the Li precursor and subsequent calcination at 700 °C under an air atmosphere, the $Ni_{1/3}Mn_{1/3}Co_{1/3}CO_3$ precursors decomposed and then formed into $LiNi_{1/3}Mn_{1/3}Co_{1/3}O_2$ (SH-NMC) with a uniform particle distribution (Fig. 2d). The final shape of the resulting SH-NMC was similar to those of $Ni_{1/3}Mn_{1/3}Co_{1/3}CO_3$ precursors. When calcined at too high temperature over 700 °C and for a long time, the nanocubes on the surface coarsely grew into larger particles. The primary particles of SH-NMC exhibited a dumbbell-like shape merged between two spherical particles with a diameter of 5 μm, as shown in Fig. 2e and g. Unlike the $Ni_{1/3}Mn_{1/3}Co_{1/3}CO_3$ precursor, nanocubes of 500–700 nm randomly oriented on the spherical core have a nodulous surface composed of nanoparticles due to the decomposition of carbonate groups and densification during calcination. The calcined nanoparticles on the facet of nanocubes ranged from 20 nm to 40 nm (Fig. 2h). Fig. 2i shows the interplanar distance and the corresponded diffraction patterns of the SH-NMC sample. The interplanar distance of SH-NMC is approximately 4.77 Å, which is in agreement with that of the (003) plane of the $LiNi_{1/3}Mn_{1/3}Co_{1/3}O_2$ phase. The high crystallinity of SH-NMC was confirmed from the distinct spot patterns obtained by the fast Fourier transform (FFT) results shown in inset of Fig. 2i. To confirm the homogenous atomic distributions of Mn, Co, and Ni in the dumbbell-shaped SH-NMC particles, EDS mapping analysis of the inset of Fig. 2j was carried out. Each element was uniformly dispersed throughout the whole region of the particle. In addition, the atomic percent of each element in SH-NMC was directly confirmed by inductively coupled plasma (ICP) mass spectroscopy. The atomic ratio among Ni, Mn, and Co was exactly 1:1:1. The results demonstrate that the exact amount of multiple transition metal components that were homogenously mixed in a carbonate precursor helped to form a single $LiNi_{1/3}Mn_{1/3}Co_{1/3}O_2$ phase without partial formation of nonstoichiometric MO_x impurities (M = Li, Ni, Mn, Co). In addition, unlike $Ni_{1/3}Mn_{1/3}Co_{1/3}CO_3$ precursors prepared by the co-precipitation method, which is based on an aqueous solution, hydrate groups absorbed on the metal carbonates were not observed from $Ni_{1/3}Mn_{1/3}Co_{1/3}CO_3$ precursors prepared by the solvo/hydrothermal method because a high proportion of organic ethylene glycol (56 v/v %) in the solution prevented the formation of hydrate carbonate (Fig. S1).

Fig. 3 shows X-ray diffraction patterns of the as-prepared $Ni_{1/3}Mn_{1/3}Co_{1/3}CO_3$ precursor and calcined $LiNi_{1/3}Mn_{1/3}Co_{1/3}O_2$ cathode material. The diffraction patterns of the $Ni_{1/3}Mn_{1/3}Co_{1/3}CO_3$ precursor were indexed as a typical carbonate structure (Fig. 3a). However, the split of each peak mainly comprising a small peak at the low angle and a large peak at the high angle from the main peak position was observed. This phenomenon is not observed in the case of co-precipitated $Ni_{1/3}Mn_{1/3}Co_{1/3}CO_3$ precursor, as shown in Fig. S2a [18]. Unlike the co-precipitated $Ni_{1/3}Mn_{1/3}Co_{1/3}CO_3$ precursor, the crystallinity of $Ni_{1/3}Mn_{1/3}Co_{1/3}CO_3$ precursor prepared by the solvo/hydrothermal method was increased, and consequently each carbonate phase was split. This result indicates that the crystalline growth of carbonate phases could be accelerated by solvo–hydrothermal reaction with high pressure and relatively high temperature compared with co-precipitation reaction occurring at ambient room temperature. Small peaks positioned at a relatively low angle (2θ) are close to the $MnCO_3$ phase (JCPDS no. 83-1763), and large peaks positioned at a relatively high angle are close to the $CoCO_3$ (JCPDS no. 11-0692) and $NiCO_3$ (JCPDS no. 78-0210) phases, respectively. Although the split of carbonate peaks was found, the atomic distribution of Ni, Mn, and Co in the carbonate particle seems to be uniform from the EDS mapping and ICP-mass results. Finally, Fig. 3b shows the diffraction patterns of the SH-NMC prepared from $Ni_{1/3}Mn_{1/3}Co_{1/3}CO_3$ precursor. The diffraction pattern of the $LiNi_{1/3}Mn_{1/3}Co_{1/3}O_2$ cathode was indexed on the basis of a hexagonal α-$NaFeO_2$ structure with the space group $R\bar{3}m$, and also showed good crystallization without any impurity phase. The specific surface area of SH-NMC and C-NMC was measured by Brunauer–Emmet–Teller (BET) analysis to examine the relationship between the number of reaction areas for Li and the kinetic properties. The surface area of the SH-NMC ($\sim$9.2 $m^2\ g^{-1}$) was two times higher than that of C-NMC ($\sim$4.4 $m^2\ g^{-1}$).

The electrochemical properties of the SH-NMC were investigated to evaluate the advantage as a cathode material compared with C-NMC prepared via the co-precipitation method. The 1st charge/discharge curves of the SH-NMC and C-NMC cathodes are shown in Fig. 4a. Typical charge/discharge curves of each $LiNi_{1/3}Mn_{1/3}Co_{1/3}O_2$ cathodes were observed without an additional plateau. The extraction and insertion of Li^+ during charging and discharging, respectively, occur in the sloping region between 3.6 V and 4.5 V due to the redox reaction of Ni and Co components [31]. The derivative capacity–voltage (dQ/dV) plots converted from Fig. 4a clearly explain the nature of the charging/discharging processes, as shown in Fig. 4b. The broad peak between 3.7 V and 4.2 V on the 1st charge in the curves is related to the oxidation of Ni ions ($Ni^{2+} \rightarrow Ni^{4+}$) and Co ions ($Co^{3+} \rightarrow Co^{4+}$), indicating the extraction

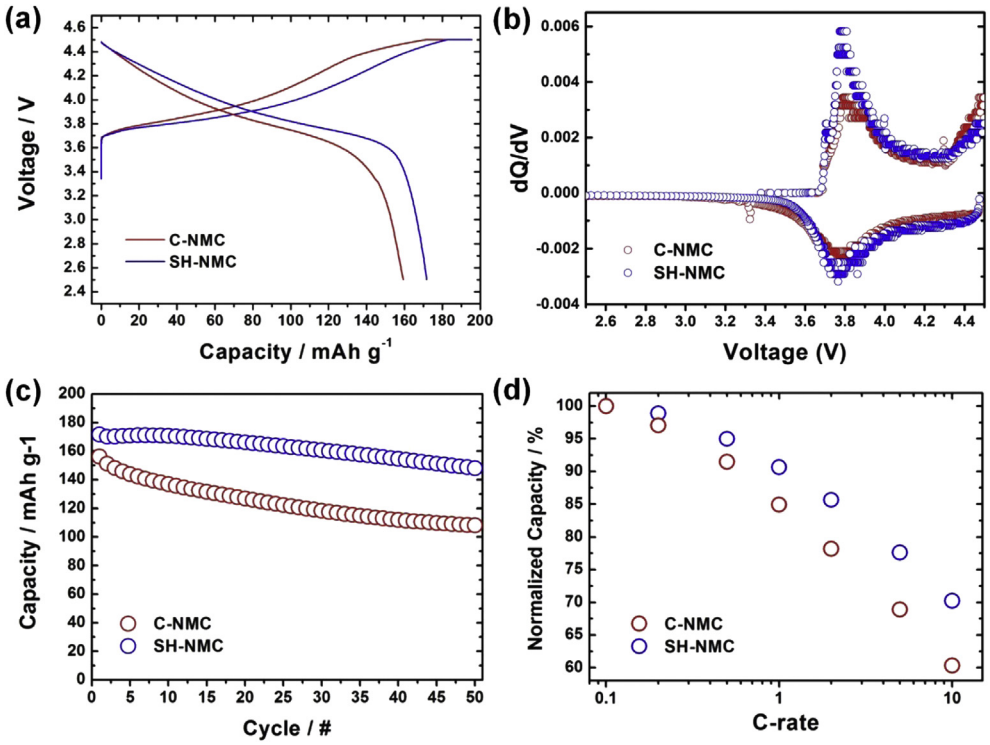

Fig. 4. (a) 1st charge/discharge curves of $LiNi_{1/3}Mn_{1/3}Co_{1/3}O_2$ prepared via urea assisted solvo/hydrothermal method (SH-NMC) and co-precipitation (C-NMC); (b) d*Q*/d*V* plots for the 1st cycle converted from (a); (c) cycle performance of the $LiNi_{1/3}Mn_{1/3}Co_{1/3}O_2$ prepared via urea assisted solvo/hydrothermal method (SH-NMC) and co-precipitation (C-NMC) for 50 cycles; (d) rate capability of $LiNi_{1/3}Mn_{1/3}Co_{1/3}O_2$ prepared via urea assisted solvo/hydrothermal method (SH-NMC) and co-precipitation (C-NMC) at different current rate from 0.1 C to 10 C. All electrochemical experiments were carried out in a voltage window between 2.5 V and 4.5 V in a constant-current condition at a current density of 16 mA g^{-1} (0.1 C, 1C = 160 mA g^{-1}) and a constant voltage at 4.5 V for 3 h during charging except for rate capability tests.

of Li^+ from the $LiNi_{1/3}Mn_{1/3}Co_{1/3}O_2$ component [32,33]. On the 1st discharge, the reduction peak around the similar potential region was found, indicating the reduction of Ni ions ($Ni^{4+} \rightarrow Ni^{2+}$) and Co ions ($Co^{4+} \rightarrow Co^{3+}$) corresponding to reverse lithium insertion into the layered structure. Mn ions are inactive in the $LiNi_{1/3}Mn_{1/3}Co_{1/3}O_2$ structure because the oxidation number of Mn is 4. Therefore, a peak at 3.4 V known to represent the redox potential of Mn was not found in the d*Q*/d*V* plot.

The specific capacity and cyclic performance of the SH-NMC have been compared with those of C-NMC, as shown in Fig. 4a and c. The 1st charge and discharge capacities of the SH-NMC electrode (charge: 196 mAh g^{-1}, discharge: 171 mAh g^{-1}) were higher than those of C-NMC electrode (charge: 185 mAh g^{-1}, discharge: 159 mAh g^{-1}). In addition, the coulombic efficiency of SH-NMC and C-NMC in the 1st cycle is estimated as 87.2% and 85.9%, respectively. In the case of the SH-NMC electrode, a high discharge capacity of 150 mAh g^{-1} after 50 cycles (87.7% of the 1st discharge capacity) was observed. In contrast, the discharge capacity of C-NMC was 108 mAh g^{-1} after 50 cycles (67.9% of 1st discharge capacity). The unique morphologies of SH-NMC, which contains dumbbell-shaped particles assembled by nanocubes, can be attributed to the further higher specific capacity and cyclic performance of SH-NMC compared with C-NMC. Fig. 4d shows the rate capability of both SH-NMC and C-NMC electrodes with increasing discharge rates from 0.1 C to 10 C (1 C = 160 mA g^{-1}). The difference in the specific discharge capacity between the SH-NMC and C-NMC electrodes becomes larger with an increasing discharge rate. The discharge capacity of the SH-NMC electrode at a high current density (1600 mA g^{-1}, 10 C) was retained at 70.2% (~120 mAh g^{-1}) of the discharge capacity at a low current density of 16 mA g^{-1} (0.1 C). In contrast, the discharge capacity of the C-NMC electrode at a high current density (1600 mA g^{-1}) is 60.3% (~96 mAh g^{-1}) of the discharge capacity at a current density of 16 mA g^{-1}. The results demonstrate that the transition metal precursors prepared via different synthesis routes can effectively affect not only the final morphologies but also the electrochemical performance of the $LiNi_{1/3}Mn_{1/3}Co_{1/3}O_2$ cathode. Manipulating the nodular surface of microsphere particles can significantly improve their kinetic properties and reactivity with Li^+ [22]. In the case of SH-NMC, many nanocubes randomly orientated on the surface of the dumbbell-shaped particles provide the innumerable Li reaction sites. To compare the reversibility of those samples, the voltage difference of each oxidation/reduction peak was estimated. The SH-NMC electrode exhibits an excellent reversibility corresponding to the low-voltage difference of the peaks (ΔV), 0.0084 V, between charging and discharging. However, the ΔV for the C-NMC is 0.1062 V. This is in good agreement with the electrochemical results from both samples.

4. Conclusions

In conclusion, the 3-D dumbbell-like $LiNi_{1/3}Mn_{1/3}Co_{1/3}O_2$ cathode material assembled with nano-building blocks was successfully synthesized from similarly shaped multicomponent carbonate precursors. The micrometer-sized, combined spherical $Ni_{1/3}Mn_{1/3}Co_{1/3}CO_3$ particles that have randomly assembled nanocubes on the surface were obtained from the urea-assisted solvo/hydrothermal method. During this synthesis process, the partial addition of viscous ethylene glycol in aqueous solution seems to play an important role, not only in suppressing the sudden particle growth but also in regulating the directional crystallization of carbonate particles on the surface. The unique hierarchical $LiNi_{1/3}Mn_{1/3}Co_{1/3}O_2$ prepared via the urea-assisted solvo/hydrothermal method exhibited better electrochemical characteristics, such as initial

discharge capacity, cyclic performance, and rate-capability as a cathode material of Li-ion batteries, compared with the $LiNi_{1/3}Mn_{1/3}Co_{1/3}O_2$ materials prepared via the conventional co-precipitation method. We hope that the multicomponent carbonate precursors prepared using our synthesis method can facilitate the preparation of diverse electrode materials for energy storage systems.

Acknowledgments

This work was supported by the Center for Inorganic Photovoltaic Materials (no. 2012-0001167) grant funded by the Korea Government (MSIP). This research was also supported by the Basic Science Research Program through the National Research Foundation of Korea (NRF), which is funded by the Ministry of Education, Science and Technology (NRF-2010-0024752). This work was also funded by the BK21 Program of the Korea Ministry of Knowledge Economy.

Appendix A. Supplementary data

Supplementary data related to this article can be found at http://dx.doi.org/10.1016/j.jpowsour.2014.02.003.

References

[1] J.M. Tarascon, M. Armand, Nature 414 (2001) 359–367.
[2] F.Y. Cheng, J. Liang, Z.L. Tao, J. Chen, Adv. Mater. 23 (2011) 1695–1715.
[3] M. Armand, J.M. Tarascon, Nature 451 (2008) 652–657.
[4] V. Etacheri, R. Marom, R. Elazari, G. Salitra, D. Aurbach, Energy Environ. Sci. 4 (2011) 3243–3262.
[5] M.S. Whittingham, Chem. Reviews 104 (2004) 4271–4301.
[6] J.B. Goodenough, K.S. Park, J. Am. Chem. Soc. 135 (2013) 1167–1176.
[7] J.B. Goodenough, Y. Kim, Chem. Mater. 22 (2010) 587–603.
[8] B.L. Ellis, K.T. Lee, L.F. Nazar, Chem. Mater. 22 (2010) 691–714.
[9] K.S. Kang, Y.S. Meng, J. Breger, C.P. Grey, G. Ceder, Science 311 (2006) 977–980.
[10] N. Recham, J.N. Chotard, L. Dupont, C. Delacourt, W. Walker, M. Armand, J.M. Tarascon, Nat. Mater. 9 (2010) 68–74.
[11] M.M. Thackeray, S.H. Kang, C.S. Johnson, J.T. Vaughey, R. Benedek, S.A. Hackney, J. Mater. Chem. 17 (2007) 3112–3125.
[12] K.M. Shaju, P.G. Bruce, Adv. Mater. 18 (2006) 2330.
[13] S.H. Kang, J. Kim, M.E. Stoll, D. Abraham, Y.K. Sun, K. Amine, J. Power Sources 112 (2002) 41–48.
[14] N. Yabuuchi, T. Ohzuku, J. Power Sources 119 (2003) 171–174.
[15] P. He, H.J. Yu, D. Li, H.S. Zhou, J. Mater. Chem. 22 (2012) 3680–3695.
[16] M.H. Lee, Y. Kang, S.T. Myung, Y.K. Sun, Electrochim. Acta 50 (2004) 939–948.
[17] C. Deng, S. Zhang, L. Ma, Y.H. Sun, S.Y. Yang, B.L. Fu, F.L. Liu, Q. Wu, J. Alloys Compd. 509 (2011) 1322–1327.
[18] T.H. Cho, S.M. Park, M. Yoshio, T. Hirai, Y. Hideshima, J. Power Sources 142 (2005) 306–312.
[19] T.H. Cho, Y. Shiosaki, H. Noguchi, J. Power Sources 159 (2006) 1322–1327.
[20] G.T.K. Fey, R.F. Shiu, V. Subramanian, J.G. Chen, C.L. Chen, J. Power Sources 103 (2002) 265–272.
[21] Y. Xu, G. Chen, E.G. Fu, M. Zhou, M. Dunwell, L. Fei, S.G. Deng, P. Andersen, Y.Q. Wang, Q.X. Jia, H.M. Luo, RSC Adv. 3 (2013) 18441–18445.
[22] W.H. Ryu, J.Y. Eom, R.Z. Yin, D.W. Han, W.K. Kim, H.S. Kwon, J. Mater. Chem. 21 (2011) 15337–15342.
[23] Y.M. Liu, F. Cao, B.L. Chen, X.Z. Zhao, S.L. Suib, H.L.W. Chan, J.K. Yuan, J. Power Sources 206 (2012) 230–235.
[24] L. Zhou, D.Y. Zhao, X.W. Lou, Angew. Chem. Int. Ed. 51 (2012) 239–241.
[25] J. Cho, J. Mater. Chem. 18 (2008) 2257–2261.
[26] J.Y. Luo, H.M. Xiong, Y.Y. Xia, J. Phys. Chem. C. 112 (2008) 12051–12057.
[27] Z.D. Huang, X.M. Liu, S.W. Oh, B.A. Zhang, P.C. Ma, J.K. Kim, J. Mater. Chem. 21 (2011) 10777–10784.
[28] J.L. Li, C.B. Cao, X.Y. Xu, Y.Q. Zhu, R.M. Yao, J. Mater. Chem. A 1 (2013) 11848–11852.
[29] S. Ashoka, G. Nagaraju, K.V. Thipperudraiah, G.T. Chandrappa, Mater. Res. Bull. 45 (2010) 1736–1740.
[30] L. Zhou, D.Y. Zhao, X.W. Lou, Adv. Mater. 24 (2012) 745.
[31] Z.X. Wang, Y.C. Sun, L.Q. Chen, X.J. Huang, J. Electrochem. Soc. 151 (2004) A914–A921.
[32] B.J. Hwang, Y.W. Tsai, D. Carlier, G. Ceder, Chem. Mater. 15 (2003) 3676–3682.
[33] Y. Koyama, I. Tanaka, H. Adachi, Y. Makimura, T. Ohzuku, J. Power Sources 119 (2003) 644–648.